



# Kinetics and physical analyses for pyrolyzed Egyptian agricultural and woody biomasses: effect of microwave drying

Mahmoud Amer<sup>1,2</sup> · Mohamed Nour<sup>3,4</sup> · Mahmoud Ahmed<sup>5</sup> · Ibrahim El-Sharkawy<sup>5</sup> · Shinichi Ookawara<sup>6</sup> · Sameh Nada<sup>4,5</sup> · Ahmed Elwardany<sup>1,2</sup>

Received: 28 November 2019 / Revised: 31 January 2020 / Accepted: 11 March 2020 / Published online: 26 March 2020  
© Springer-Verlag GmbH Germany, part of Springer Nature 2020

## Abstract

This paper investigates microwave drying effect as a pretreatment method on the kinetic parameters of four torrefied biomasses. The considered biomasses are rice straw, rice husk, sugarcane, and cotton stalks. Dried samples (microwave or oven-dried) were then torrefied under isothermal conditions in a thermogravimetric analyzer (TGA) at two different temperatures of (250 and 300 °C). Two simple kinetics methods were applied including direct Arrhenius (DA) and Coats and Redfern (CR). The physical structure of rice straw and cotton stalks as a function of drying method and torrefaction temperature has been studied using Brunauer–Emmett–Teller (BET) surface area technique. Results revealed that microwave drying increased both the activation energy and the pre-exponential factor for both rice straw and sugarcane regardless of the torrefaction temperature, while the opposite occurred for rice husk. In the case of cotton stalks, microwave drying increased the kinetic parameters at 250 °C and decreased them at 300 °C. The activation energy and pre-exponential factor values obtained from CR method were larger than the ones from DA method. The 300 °C torrefied, conventionally dried rice straw has the lowest activation energy and pre-exponential factor and the largest peak width indicating wide range of reactivity. While microwave dried sugarcane, torrefied at 250 °C, is the hardest one to react. All microwave dried samples require more heat to decompose regardless of the torrefaction temperature. Microwave drying increased the surface area, mean pore diameter, and pore volume for rice straw, while the opposite occurred for cotton stalks due to its woody nature.

**Keywords** Pyrolysis kinetics · Biochar · Torrefaction · Microwave drying

✉ Ahmed Elwardany  
ahmed.elwardany@ejust.edu.eg; ahmed.elwardany@alexu.edu.eg

<sup>1</sup> Fuels and Combustion Engines Laboratory, Energy Resources Engineering Department, Egypt-Japan University of Science and Technology (E-JUST), New Borg El-Arab City, Alexandria 21934, Egypt

<sup>2</sup> Mechanical Engineering Department, Faculty of Engineering, Alexandria University, Alexandria 21544, Egypt

<sup>3</sup> School of Mechanical Engineering, Shanghai Jiao Tong University, Dongchuan Road 800 Shanghai 200240, China

<sup>4</sup> Mechanical Engineering Department, Benha Faculty of Engineering, Benha University, Benha, Qalubia 13512, Egypt

<sup>5</sup> Energy Resources Engineering Department, Egypt-Japan University of Science and Technology (E-JUST), New Borg El-Arab City, Alexandria 21934, Egypt

<sup>6</sup> Department of Chemical Science and Engineering, Tokyo Institute of Technology, Tokyo 152-8552, Japan

## Nomenclature

TGA	Thermogravimetric analyzer
CR	Coats and Redfern
QCD	Carbon quantum dots
CD	Conventional drying
FWO	Flynn-Wall-Ozawa
DSC	Differential scanning calorimetry
RH	Rice husk
CS	Cotton stalks
HHV	Higher heating value
E	Activation energy
t	Time
DA	Direct Arrhenius
BET	Brunauer–Emmett–Teller
MWD	Microwave drying
AEDM	Activation energy distribution model
DTA	Differential thermal analysis
RS	Rice Straw

SC	Sugarcane bagasse
XRD	X-ray diffraction
A	Frequency or pre-exponential factor
T	Temperature [k]
DTG	First derivative of TG function

## 1 Introduction

Torrefied biomass (biochar) is considered as a renewable energy resource with several advantages over raw biomass. These advantages include high energy density, stability during storing, hydrophobicity, easy handling and transfer, and high grindability [1]. Biochar applications are not limited to energy; they also include soil enhancement [2], superconductors [3, 4], adsorbents [5], water purification [6], and synthesis of carbon quantum dots (QCD) [7]. Many research efforts have been conducted on torrefaction for different types of biomasses including agriculture and agro-food industries wastes [8–15]. Particularly, this includes optimization of the torrefaction process for biomass, effect of co-pyrolysis of different biomasses/wastes, morphology and structural analyses of biochar, and kinetics of biochar pyrolysis and combustion. The latter is significantly important for modeling and simulation activities of biochar/biomass combustion [16].

It is well-known that dielectric materials are heated up when high frequency (Microwave) electromagnetic waves are applied to them. The electric field polarizes dipolar molecules and moves ionic charges within the dielectric materials [17]. One of the most polar materials that gets profoundly affected by microwaves is water represented in the biomass' moisture content [17, 18]. Microwave has evoked massive research interest because it reduces the operating time. Microwave usage has a crucial disadvantage regarding the high electrical cost of running it continuously. This drawback led to using microwaves only for a short time as a pretreatment, specifically drying. After the pretreatment, a more efficient conventional process could take place [17]. In a previous study by the authors [19], the effects of microwave drying (MWD) and conventional drying (CD) at 105 °C on the dry torrefaction of rice straw, rice husk, sugarcane, and cotton stalks have been investigated. The torrefaction was performed at 250 and 300 °C [19]. It was found that the drying time was more than 60 times faster with microwave. Also, the violent microwave drying ruptured the surface of the biomass, releasing more volatiles than their respective conventionally dried samples. The torrefied microwave dried rice straw, rice husk, and sugarcane bagasse had lower crystallinity, heating value, energy yield, and carbon content. The opposite was monitored for cotton stalks.

Investigating pyrolysis kinetics is crucial to understand the overall thermochemical conversion process of biomass pyrolysis [20, 21]. The most commonly used method to obtain the kinetic parameters is the thermogravimetric analysis (TGA) [20, 22–25]. TGA could be used for proximate analysis of

solid fuels along with the determination of pyrolysis and combustion kinetics [22]. There exist numerous kinetic models to calculate the biomass' kinetic parameters grouped under two main methods which are the model-fitting method and the model-free or isoconversional method [26, 27]. In the model-fitting method, different reaction mechanisms are applied to the thermogravimetric data, and the model that gives the best fit is considered for the determination of kinetic parameters. To obtain this best fit, the reaction order is assumed, and then manipulating the rate equation until a straight-line plot can be obtained from where the remaining unknown parameters can be obtained by linear regression. This model-fitting method includes direct Arrhenius plot, Coats and Redfern, and Freeman and Carroll methods [28]. While in the model-free method, no reaction mechanism is pre-assumed, and the kinetic information is extracted by developed mathematical relations [26]. Kreutter et al. [29] performed a non-isothermal TGA analysis with nonlinear model-fitting for biosolid obtained from the water resource recovery facility.

Papari and Hawboldt [23] and Hameed et al. [30] summarized different approaches for obtaining the kinetic parameters of woody biomass using TGA. This includes global kinetic model, three parallel reactions, competitive models, models with secondary tar cracking, Shafizadeh and Bradbury model, activation energy distribution model (AEDM), chemical percolation devolatilization model, and five parallel pseudo-component  $n^{\text{th}}$  order model [29]. Cai et al. [22] stated different model-free kinetic methods including the Friedman, the Ozawa-Flynn-Wall, the Kissinger-Akahira-Sunose, the Vyazovkin, the advanced Vyazovkin, and the Cai-Chen models. Cai et al. [22] used the Friedman isoconversional kinetic method to analyze lignocellulosic biomass pyrolysis because of its simplicity and high accuracy among the model-free methods. They also included the smoothing of the derivative curve and error elimination from the TGA data.

Direct Arrhenius plot (DA) and the graphical method developed by Coats and Redfern (CR) are two commonly used model-fitting methods [26]. Many researchers used these two methods to determine the kinetic parameters for sugarcane bagasse and cotton stalks [31], microwave torrefied rice straw [32], rice and corn husks [26], heavy fuel oil [33, 34], and coal-biomass blends. Jayaraman et al. [35] utilized CR kinetic model to calculate the kinetic parameters of microalgae and Mallick et al. [36] for water hyacinth. Through the literature, it is found that many factors affect the activation energy, such as the pyrolysis temperature, kinetic analysis mathematical models, and pyrolysis techniques. As a result, the literature offers a wide range of values of activation energy for the same biomass type [31].

In a recent study by Chen et al. [37], a comparison between the effect of conventional drying at 105 °C for 20 h and microwave drying on the kinetic parameters of pyrolyzed microalgae using CR method has been conducted. It was found that microwave drying reduced both the activation

energy and the pre-exponential factor. Liang et al. [38] utilized the Flynn-Wall-Ozawa (FWO) kinetics method to obtain the kinetic parameters for the fast pyrolysis of microwave pretreated water hyacinth. The microwave pretreatment was shown to decrease the activation energy at low pretreatment times but increased when the time increased.

The differential thermal analysis (DTA) is used to measure the heat flow due to biomass thermal degradation as the differential scanning calorimetry (DSC). The thermal behavior of fly ash from Bulgarian lignite coals was investigated by DTA at different heating rates by Boycheva et al. [39]. Elsayed et al. [40] performed a kinetic study on the raw sugarcane bagasse and cotton stalks using both TGA and DTA techniques at different heating rates. Through the literature, the DTA studies on biomass analysis are very limited.

The BET Brunauer – Emmett – Teller (BET) test is used to determine the internal surface area and the pore volume of the produced biochar from the adsorption of the nitrogen. The BET surface area is important because the gasification and pyrolysis processes occur on the surface of the biochar's particles. The BET surface area plays an important role in the determination of the biochar's porosity and intrinsic reaction rate. This could make two char particles with identical external size behave differently due to their different internal structure and size [41–44]. Generally, the porous structure is an advantage in activated carbon which increases its tendency to absorb ambient moisture and in biochar when applied in soil remediation. However, the high porosity and its subsequent high moisture uptake could be a disadvantage when the biochar is used as fuel which may degrade its quality [45].

This work is complementary to the authors' previous work [19] to investigate the effect of the different initial drying pretreatment methods, conventional and microwave, on the kinetic parameters, and the physical structure of biochar samples. Two simple kinetics approaches are used, namely, DA and CR for this investigation along with BET analysis. Both DA and CR utilize a single heating rate TGA curve to generate the kinetic results, and they both result the same trend in most cases, so a comparison is to be performed between their results.

## 2 Methodology

### 2.1 Materials

Four torrefied biomasses namely rice straw (RS), rice husk (RH), sugarcane bagasse (SC), and cotton stalks (CS) were considered. They were produced from the previous work of the authors [19]. Each one of these samples undergone conventional drying (CD) and microwave drying (MWD) with their subsequent mild and severe torrefaction for 30 min at 250 °C and 300 °C, respectively. This combination of

torrefaction after drying results in 16 samples which were milled and prepared for analyses. To easily address each sample, their name will comprise of 3 parts separated by dashes through the rest of this article. The first is the biomass type RH, RS, SC, or CS. The second is the drying method, either CD or MWD. The third is the torrefaction temperature, either 250 °C or 300 °C.

Proximate, ultimate, higher heating value, mass and energy yields, XRD crystallinity, and SEM measurements have been performed for all of 16 samples and presented in Amer et al. [19]. The results showed that sugarcane, rice husk, and cotton stalk have the most promising values of elemental carbon, energy yield, and heating value. Severely torrefied rice straw showed the highest crystallinity values of 50.7% and 27.17% for conventional and microwave dried samples, respectively. Sugarcane and rice husk were shown to be completely amorphous. The severely torrefied samples at 300 °C always show larger increase in higher heating value (HHV) than their respective mildly torrefied ones at 250 °C regardless of the drying method. The HHV for the severely torrefied conventionally dried samples are 32.31, 31.17, 29.73, and 27.71 MJ/kg for SC, RH, RS, and CS, respectively. While the HHV for the severely torrefied microwave dried samples are 29.7, 29.05, 28.77, and 27.4 MJ/kg for CS, RH, SC, and RS, respectively. The woody nature of CS makes it produce a microwave pretreated biochar having higher HHV and energy yield compared to the conventionally dried ones.

### 2.2 TGA, DTG, and DTA analyses

The TGA and DTA were conducted using Setaram LABSYS-evo-TG/DSC/DTA simultaneous thermal analyzer which can reach a maximum temperature of 1600 °C with a heating rate from 0.01 to 100 °C/min. The non-isothermal TGA experiments are performed with 100 ml/min of high purity argon (99.99%) as a carrier and a constant heating rate of 40 °C/min. The TGA analysis is performed using the TGA rod with a single large crucible, while the DTA analysis uses a two-crucible rod, one for the tested sample, while the other is empty for reference with the heat flow sensor placed in between. For DTA, the primary measuring signal during a measurement is the temperature difference between a sample and reference in  $\mu\text{V}$  (thermal voltage). As the used thermal analyzer have DTA and DSC capabilities, then the temperature difference can be converted to heat flow in (mW) by appropriate calibration. The same temperature profile was used for both TGA and DTA tests.

### 2.3 Kinetic parameters study

The thermal decomposition of biomass is governed by the following equation [31]:

$$\frac{d\alpha}{dt} = k f(\alpha) \quad (1)$$

where  $\alpha$  and  $\frac{d\alpha}{dt}$  are the normalized form for mass loss and its first derivative.  $k$  is the temperature-dependent rate constant, and  $f(\alpha)$  is the conversion function which depends on the reaction's mechanism. The previous equation depicts that the rate of reaction is a function of the mass conversion ratio  $\alpha$  in time  $t$ .  $\alpha$  and  $\frac{d\alpha}{dt}$  are expressed by the following equations:

$$\alpha = \frac{m_i - m_t}{m_i - m_f}, \quad (2)$$

$$\frac{d\alpha}{dt} = \frac{-1}{m_i - m_f} \frac{dm_t}{dt}, \quad (3)$$

where  $m_i$ ,  $m_f$ , and  $m_t$  are the initial, final, and instantaneous mass of the sample at the beginning, end, and any time ( $t$ ) of the reaction peak in mg.  $f(\alpha)$  is a function of the reaction's mechanism which depends on the type of the sample being studied. For biomasses, the reaction is  $n^{\text{th}}$  order as shown in the following equation:

$$f(\alpha) = (1 - \alpha)^n, \quad (4)$$

where  $n$  is the order of the reaction. This  $n^{\text{th}}$  order reaction is the most common form and it indicates that the reaction rate is proportional to the reactants left to react.

$k$  (Eq. (1)) represents the temperature-dependent rate constant which is described by the following Arrhenius equation [29, 46] as:

$$k = A e^{-E/RT}, \quad (5)$$

where  $A$  is the frequency or the pre-exponential factor in  $\text{min}^{-1}$ ,  $E$  is the decomposition reaction's apparent activation energy in kJ/mol,  $R$  is the universal gas constant in kJ/mol.  $K$  and  $T$  is the temperature in K.

Substituting Eqs. (5) and (4) into Eq. (1) gives the following reaction rate expression:

$$\frac{d\alpha}{dt} = A e^{-E/RT} (1 - \alpha)^n \quad (6)$$

As this is a non-isothermal TGA experiment with a linear heating rate, where  $\beta$  is expressed by the following equation [31]:

$$\beta = \frac{dT}{dt} \quad (7)$$

The rate of change of the conversion ratio is expressed relative to temperature  $T$  as follows:

$$\frac{d\alpha}{dT} = \frac{d\alpha}{dt} \times \frac{dt}{dT}. \quad (8)$$

Substituting eqs. (6) and (7) into eq. (8), the following equation is obtained:

$$\frac{d\alpha}{dT} = \frac{A}{\beta} e^{-E/RT} (1 - \alpha)^n. \quad (9)$$

Equation (9) represents the fraction of material decomposed in the given peak interval. In this work, two kinetic models were applied to calculate the kinetic parameters  $E$ ,  $A$ , and  $n$  for the studied samples, namely, direct Arrhenius plot (DA) [35] and the integral graphical method developed by Coats and Redfern (CR) [47, 48]. Both methods depend on the principle of fitting a curve with a straight line having the basic following equation:

$$Y = mX + c, \quad (10)$$

where  $m$  is the slope of the line and  $c$  is the intersection with the  $y$ -axis.

To determine the kinetic parameters, the DTG peaks need to be determined first from the TGA/DTG results. Then the following calculations are performed across the peak's range only [31].

### 2.3.1 Direct Arrhenius plot

In this method, the logarithm is taken for both sides of Eq. (9) which results in the following equation:

$$\ln \left\{ \frac{1}{(1 - \alpha)^n} \times \frac{d\alpha}{dT} \right\} = \ln \left\{ \frac{A}{\beta} \right\} - \frac{E}{R} \times \frac{1}{T}. \quad (11)$$

By comparing Eq. (10) and Eq. (11), the relation between  $Y = \ln \left\{ \frac{1}{(1 - \alpha)^n} \times \frac{d\alpha}{dT} \right\}$  and  $X = \frac{1}{T}$  could be plotted. To determine the correct reaction order, various values of  $n$  were taken ranging from 0.1 to 1.5 with a 0.1 incrementation, and plots of  $Y$  versus  $X$  for all values of  $n$  were obtained. All plots were straight lines fitted, and the best fit line was selected having the highest  $R^2$  value. Then the slope of this line  $= -\frac{E}{R}$ , from which the activation energy ( $E$ ) could be obtained. Also, the  $y$ -axis intercept equals  $c = \ln \left\{ \frac{A}{\beta} \right\}$  from which the frequency factor ( $A$ ) is obtained.

### 2.3.2 Integral graphical method (CR)

Coats and Redfern developed this method to obtain the kinetic parameters from the following modified equations [47, 48]:

$$A = \pi r^2 \ln \left\{ \frac{1 - (1 - \alpha)^{1-n}}{T^2 (1-n)} \right\} \\ = \ln \left\{ \frac{AR}{\beta E} \times \left( 1 - \frac{2RT}{E} \right) \right\} - \frac{E}{R} \times \frac{1}{T} \quad \text{for } n \neq 1, \quad (12)$$

$$\ln\left\{\frac{-\ln(1-\alpha)}{T^2}\right\} = \ln\left\{\frac{AR}{\beta E} \times \left(1 - \frac{2RT}{E}\right)\right\} - \frac{E}{R} \times \frac{1}{T} \quad \text{for } n = 1 \quad (13)$$

Eqs. (12) and (13) could be simplified because  $\frac{2RT}{E} \ll 1$ , making  $1 - \frac{2RT}{E} \approx 1$  thus both Eqs. (12) and (13) could be re-written as follows [31, 36]:

$$\ln\left\{\frac{1-(1-\alpha)^{1-n}}{T^2(1-n)}\right\} = \ln\left\{\frac{AR}{\beta E}\right\} - \frac{E}{R} \times \frac{1}{T} \quad \text{for } n \neq 1 \quad (14)$$

$$\ln\left\{\frac{-\ln(1-\alpha)}{T^2}\right\} = \ln\left\{\frac{AR}{\beta E}\right\} - \frac{E}{R} \times \frac{1}{T} \quad \text{for } n = 1 \quad (15)$$

By comparing Eqs. (14) and (15) with Eq. (10), a relation between  $Y = \ln\left\{\frac{1-(1-\alpha)^{1-n}}{T^2(1-n)}\right\}$  for  $n \neq 1$  or  $Y = \ln\left\{\frac{-\ln(1-\alpha)}{T^2}\right\}$  for  $n = 1$  and  $X = \frac{1}{T}$  could be plotted, and the order of reaction will be determined as well by trying the  $n$  values ranging from 0.1 to 2.5 with 0.1 incrementation. The value of  $n$  changed from DA to CR because it is obtained by trial and error based on the best fit line which has the highest  $R^2$  value. As the CR equations differed from the DA equations, the best fit lines changed resulting in higher values of  $n$ . The same steps will be performed as with the direct Arrhenius method to get the line with the best  $R^2$  value. Then the slope of this line  $= -\frac{E}{R}$ , from which the activation energy ( $E$ ) could be extracted. The  $y$ -axis intercept equals  $c = \ln\left\{\frac{AR}{\beta E}\right\}$  from which the frequency factor ( $A$ ) is obtained. The activation energy and the frequency factor represent the reaction’s velocity which depends on the temperature ( $T$ ), conversion ( $\alpha$ ), and time ( $t$ ) from the TGA data [21, 22].

### 2.4 BET analysis

The studied four biomasses represent two different categories: agricultural and woody biomasses. The agricultural biomass includes RS, RH, and SC. The woody biomass includes the CS. Following the results reported in the previous study [19], it was found that CS behavior in response to MWD is opposite to the other 3 biomasses. Hence, RS and CS are selected for the BET surface area and pore volume test to represent the agricultural and the woody biomasses, respectively. The torrefied samples for RS and CS are finely milled as a preparation for the BET BELSORP surface area analyzer device. This device uses liquid nitrogen and nitrogen as adsorption gas with a maximum pretreatment temperature of 400 °C and a minimum measurable specific surface area range of 0.01 m<sup>2</sup>/g. The degasification pretreatment temperature for the device is 160 °C, with an overnight incubation period before the test [49]. To investigate the effect of torrefaction temperature and MWD on the biomass’ porosity, the percentage change in BET parameters is calculated for all obtained BET parameters.

Equations (16) and (17) are for the effect of torrefaction temperature at the same drying method and for the MWD effect at the same torrefaction temperature, respectively.

$$\begin{aligned} \% \text{Change}|_{\text{Temperature}} &= \frac{\text{BET parameter}_{300} - \text{BET parameter}_{250}}{\text{BET parameter}_{250}} \times 100, \quad (16) \end{aligned}$$

$$\begin{aligned} \% \text{Change}|_{\text{MWD}} &= \frac{\text{BET parameter}_{\text{MWD}} - \text{BET parameter}_{\text{CD}}}{\text{BET parameter}_{\text{CD}}} \times 100. \quad (17) \end{aligned}$$

## 3 Results and discussion

### 3.1 Effect of drying method on the kinetic parameters

The kinetic parameters are extracted from the TGA/DTG (thermogravimetric analysis/first derivative of thermogravimetric function) curves provided in the authors’ previous work [19].

A sample calculation curve for these kinetic characteristic parameters along with DDTG (Second derivative of thermogravimetric function) is shown in Fig. 1 for RS-MWD-250. The same calculations are made for the rest of the 16 samples.

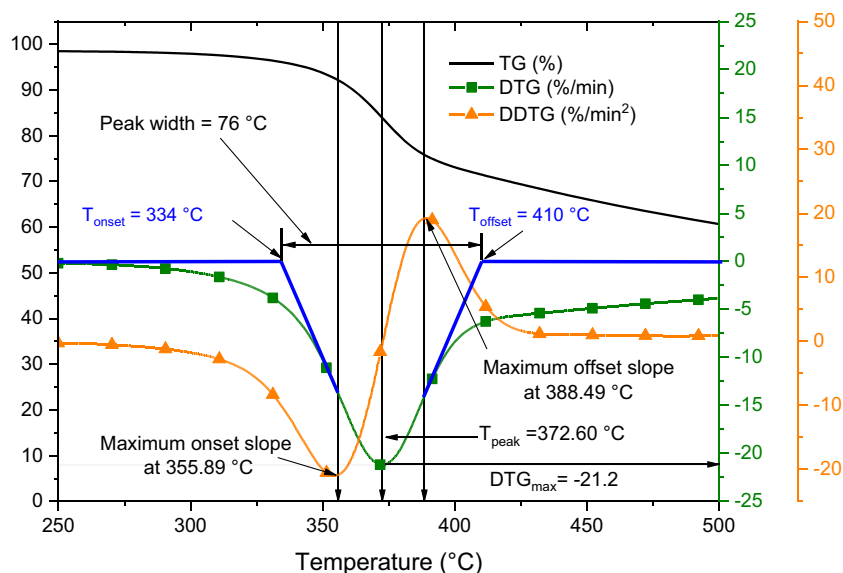
The maximum slope inflectional points at the onset and offset sides could be obtained using the peaks of the DDTG. Tangent lines are drawn to the peak width lines of DTG and their intersection with the horizontal axis results in the onset and offset temperatures, respectively. Then, the peak width could be determined. The DTG peak position defines  $T_{\text{peak}}$  and  $\text{DTG}_{\text{max}}$ .

The position of the peak on the horizontal temperature axis determines which component is decomposed. Hemicellulose decomposes between 220 and 300 °C, cellulose between 275 and 350 °C and lignin has a wider range between 160 and 900 °C [43, 50, 51].

The onset temperature, peak temperature, offset temperature, and peak width are explained according to ISO 11357-1:2010–03 standard as follows [31, 46]:

- $T_{\text{onset}}$  is the extrapolated onset temperature for the peak which is the designed intersection point of the extrapolated baseline and the inflectional tangent at the beginning of the melting or crystallization peak. The inflectional point is the point of maximum slope on the rising side of the peak which corresponds to the maximum value of the second derivative (DDTG) at the onset side.
- $T_{\text{Peak}}$  is the peak temperature which marks the point at which the largest deviation of the decomposition rate from the baseline is measured.
- $\text{DTG}_{\text{max}}$  is the maximum decomposition rate of the peak.

**Fig. 1** Sample calculation for the kinetic characteristic properties for RS-MWD-250



- $T_{\text{offset}}$  is the extrapolated offset temperature for the peak which is the designed intersection point of the extrapolated baseline and the inflectional tangent at the end of the melting or crystallization peak. The inflectional point is the point of maximum slope on the falling side of the peak which corresponds to the maximum value of second derivative (DDTG) at the offset side.
- Peak width is the temperature interval between the onset and offset temperature points.

The onset temperature is less dependent on heating rate and sample mass than the peak temperature. It should remain unchanged when the peak temperature shifts due to changing heating rate or sample preparation. Thus, this value could be used for comparison of different thermal events. The peak temperature is highly dependent on the sample crystallinity, crystal size, sample preparation, and heating rate, which makes this value unreliable for comparison. The offset temperature depends on the location of both the onset and peak temperatures. So, any change in the heating rate results in shifting the offset temperature and changes the peak's width as found in numerous results in the literature [22, 26, 29, 35, 52–54].

The kinetic characteristic properties of the samples are shown in both Figs. 2 and 3. It is shown in Fig. 2 that as the torrefaction temperature increases, the onset and offset temperatures and the peak width are increased. This indicates higher decomposition's starting and ending temperatures as along with the duration for severely torrefied samples at 300 °C.

At 250 °C torrefaction, MWD delayed the start of decomposition for RS, SC, and CS, while it made RH decompose earlier than its CD sample as shown in Fig. 2a. MWD delayed the end of decomposition for RH, SC, and CS, while a slight advance was monitored for RS as shown in Fig. 2b. The combination of the effect of MWD on the  $T_{\text{onset}}$  and  $T_{\text{offset}}$  resulted

in the shown effect in Fig. 2c for the peak width. At 250 °C, MWD was shown to have a scattered effect on peak width. While at 300 °C, MWD led to a pronounced reduction in peak width for the woody biomass (CS). This different behavior at 250 °C could be attributed to the different percentages of the hemicellulose and cellulose contents in these biomasses which only start decomposing at this temperature. However, at 300 °C torrefaction, all hemicellulose is to be decomposed, and cellulose starts decomposing which results in a consistent result for all biomasses. In conclusion, MWD decreased the onset and offset temperatures as well as the peak width for all biomasses which are torrefied at 300 °C.

Both mildly torrefied (250 °C) RS and CS have the highest values of peak width. This shows that although they start and end the decomposition stage earlier than the other two biomasses, they take longer time and temperature range to decompose. This indicates that RS and CS contain higher remaining levels of crystalline cellulose which is easier to decompose and lower remaining levels of amorphous lignin after the torrefaction at 250 °C. This agrees with the previous results which revealed that RS and CS have higher crystallinity values than RH and SC at 250 °C [19].

Figure 3 shows the peak temperature and maximum decomposition rate of the peak for different torrefied biomasses conventionally and microwave dried. It is found that as the torrefaction temperature increases, the peak temperature increases, while the absolute  $\text{DTG}_{\text{max}}$  decreases, regardless of the drying method. This reduction in  $\text{DTG}_{\text{max}}$  reduces the peak's severity. This is attributed to the release of more volatiles, the almost complete decomposition of the hemicellulose, and the reduction of the remaining amounts of cellulose and lignin when severely torrefied at 300 °C [19, 55].

At 250 °C torrefaction, MWD increased both the absolute value of  $\text{DTG}_{\text{max}}$  and  $T_{\text{peak}}$  for RS, SC, and CS, while the

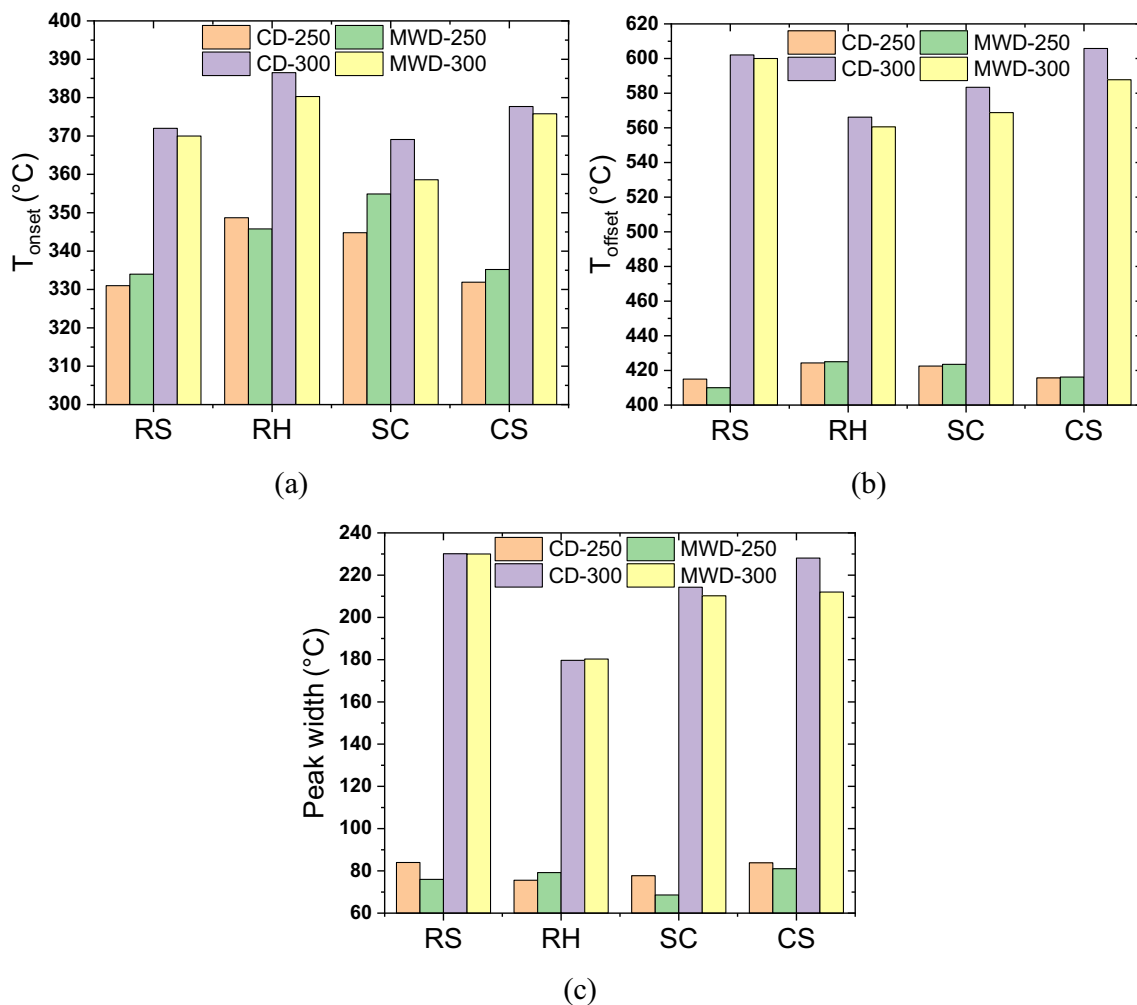


Fig. 2 The effect of MWD on  $T_{onset}$  (a),  $T_{offset}$  (b), and Peak width (c) on the torrefied biomass

opposite occurred for RH. This can be attributed to the larger particle size of the RH, as it already had initial smaller size so it wasn't ground like the other biomasses [19]. At 250 °C torrefaction, RH-MWD had a larger surface area than RH-

CD due to the violent rupturing of the inner passages from MWD which resulted in releasing more hemicellulose during the torrefaction from RH-MWD. This subsequently reduced the hemicellulose component of the peak which reduced  $T_{onset}$

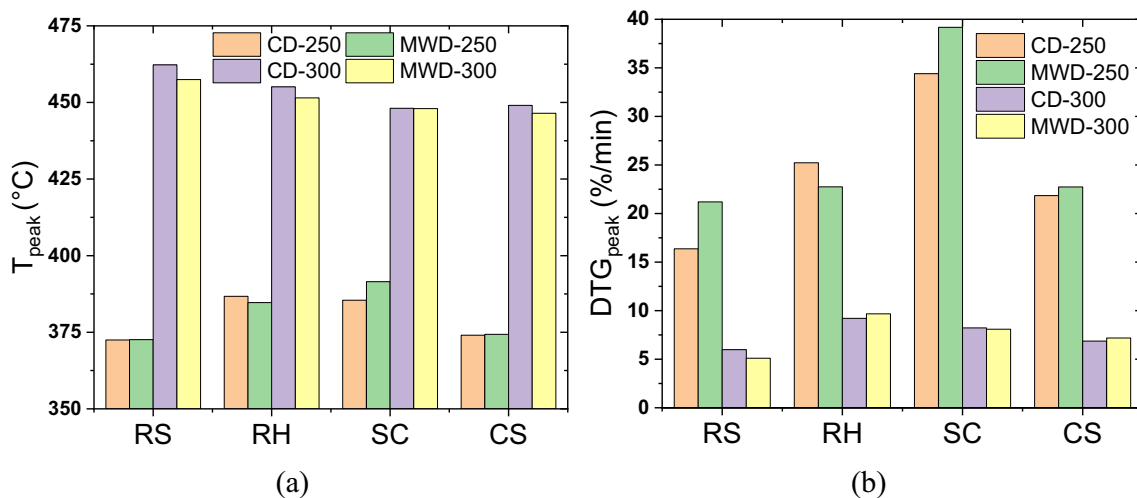


Fig. 3 The effect of MWD on (a) the peak temperature and (b) the max DTG value for the selected biomasses

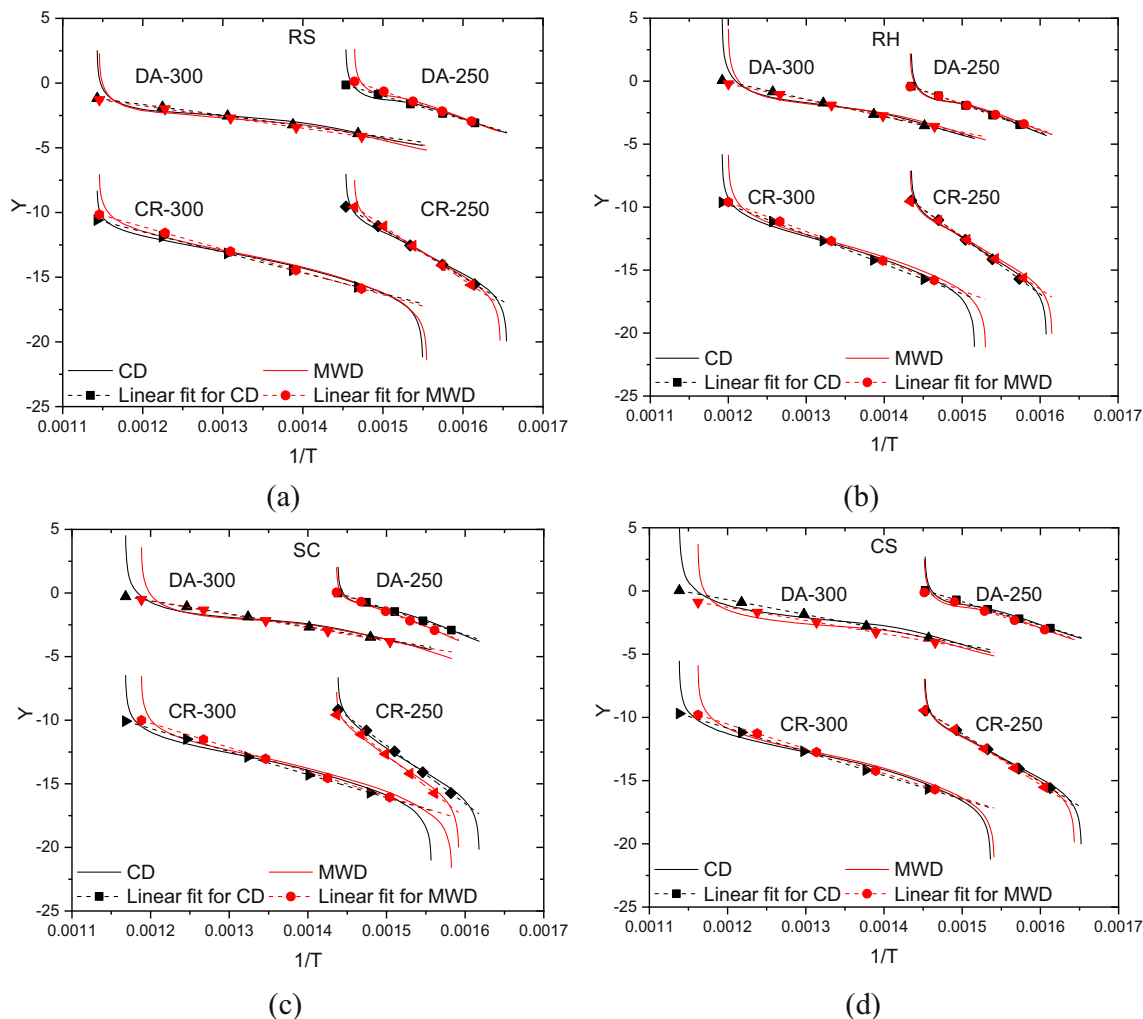
as shown in Fig. 2a and reduced  $T_{\text{peak}}$  and  $\text{DTG}_{\text{max}}$ . At 300 °C torrefaction, MWD decreased  $T_{\text{peak}}$  for all biomasses, decreased the absolute value of  $\text{DTG}_{\text{max}}$  for RS and CS only, and increased  $\text{DTG}_{\text{max}}$  for RH and SC.

Figure 4 shows the  $Y$  versus  $1/T$  for all samples with their linear fit at the value of reaction order  $n$  which has the highest  $R^2$  value using both DA and CR methods. These values of  $n$  and  $R^2$  are listed in Table 1. The reaction order that provided the best fit is in the range from 0.8 to 1.3 and from 1.7 to 2 for DA and CR methods, respectively. Torrefaction at 250 °C had reaction orders of less than one, whereas at 300 °C, the reaction order is one or more. CR method results have higher  $R^2$  values ranging between 0.943 and 0.974, while DA method has lower  $R^2$  values ranging between 0.856 and 0.967.

Figure 5 shows the kinetic properties ( $E$  and  $\ln(A)$ ) for the torrefied biomass using both the DA method as in Fig. 5a, c and the CR method as in Fig. 5b, d, respectively. The activation energy and pre-exponential factor values obtained from Coats and Redfern method are larger than their respective

values from the direct Arrhenius method which agrees with the results from the literature [26, 31–33, 35]. The values of  $E$  calculated by CR equals a minimum of 1.6 times the values using DA method for CS-CD-300 and a maximum of 2.25 times for SC-CD-250. While these values are a minimum of 1.47 for CS-CD-300 and a maximum of 2.15 for SC-CD-250 in the results of  $\ln(A)$ . It is clear from Fig. 5 that as the torrefaction temperature increases, both  $E$  and  $A$  decrease which is reasonable because the higher the torrefaction temperature, the more broken bonds by thermal treatment, the less energy required to start the reaction [37, 56].

At 250 °C torrefaction, MWD increased both  $E$  and  $A$  for RS, SC, and CS, while the opposite occurred for RH regardless of the kinetic model used. This can be attributed to the lower hemicellulose content in RH-MWD-250 than RH-CD-250 from the violent rupturing of MWD which make it have less components to devolatilize. This makes it easier to react thus having lower  $E$ . At 300 °C torrefaction and with CR method only, the above applies for all samples. While for



**Fig. 4**  $Y$ - $1/T$  curves (Eq. (11) for DA and Eq. (14) for CR) with their linear fit at the best fit  $n$  value (shown in Table 1) for (a) rice straw, (b) rice husk, (c) sugarcane bagasse, and (d) cotton stalks



**Table 1** Kinetic parameters from Arrhenius and graphical methods

Biomass	Torrefaction temp. (°C)	Drying Method	Arrhenius		Coats and Redfern	
			<i>n</i>	<i>R</i> <sup>2</sup>	<i>n</i>	<i>R</i> <sup>2</sup>
RS	250	CD	0.9	0.927	1.9	0.968
		MWD	0.9	0.946	1.8	0.974
	300	CD	1.0	0.890	1.8	0.954
		MWD	1.0	0.896	1.8	0.951
RH	250	CD	0.9	0.938	1.9	0.971
		MWD	0.9	0.929	1.9	0.969
	300	CD	1.2	0.881	2.0	0.952
		MWD	1.1	0.889	2.0	0.953
SC	250	CD	0.8	0.961	1.9	0.973
		MWD	0.8	0.967	1.7	0.976
	300	CD	1.1	0.860	1.9	0.946
		MWD	1.0	0.888	1.9	0.949
CS	250	CD	0.9	0.936	1.9	0.970
		MWD	0.9	0.931	1.9	0.971
	300	CD	1.3	0.856	2.0	0.943
		MWD	1.1	0.860	2.0	0.944

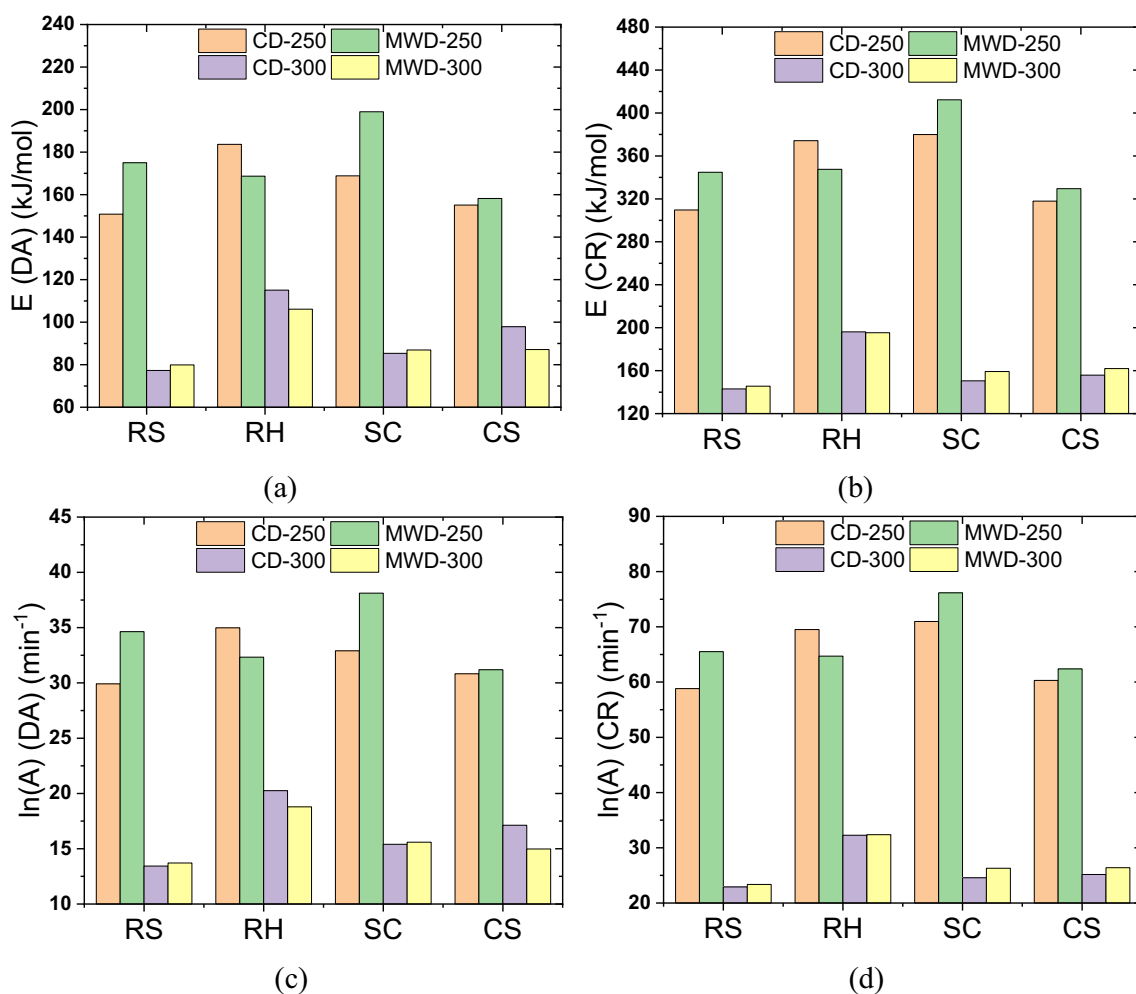


**Fig. 5** Kinetic properties (*E* and *ln(A)*) of the torrefied biomass using the DA method (a and c) and the CR method (b and d)

DA method, it applies only for RS, RH, and SC. However, for CS, MWD reduced both  $A$  and  $E$ .

RS-CD-300 has the lowest values of  $E$  and  $\ln(A)$  which are 77.3 and 143 kJ/mol, and 13.4 and 22.9 min<sup>-1</sup> according to DA and CR methods, respectively. This means that RS-CD-300 is the easiest one to react, and it requires the lowest amount of external temperature and time to start decomposing. This is attributed to the very high crystallinity of 50.79% for the RS-CD-300 extracted from [19], and it totally agrees with the work of Bhuiyan et al. [57] where they found that the more crystalline the material, the easier it reacts. Also, RS-CD-300 has the largest peak width of 230.1 °C as stated in Fig. 2. This means that it decomposes over a wide range of temperatures and has a large span making it easier to decompose. SC-MWD-250 has the maximum values of  $E$  and  $\ln(A)$  of 199 and 412.3 kJ/mol, and 38.1 and 76.2 min<sup>-1</sup> according to DA and CR methods, respectively. This indicates that it requires the highest external temperature and the longest time to react. This can be related to two reasons. The first is that it is amorphous with very low crystallinity of 4.8765%. The second is related to the elemental analysis of the SC-MWD-250. It has the second lowest amount of carbon content of 59.1% and the largest amount of oxygen content of 34.9% based on dry ash free analysis. It also has the second lowest HHV of 23.49 MJ/kg after RS-MWD-250. The low carbon and high oxygen contents make the sample less reactive thus having the highest values of activation energy and pre-exponential constant. Also, SC-MWD-250 has the lowest peak width of 68.6 °C only as shown in Fig. 2. This indicates that it decomposes over a very narrow temperature range making it harder to decompose.

The data from Fig. 2 and Fig. 5 can be correlated together relating the activation energy with the peak width. They show that as the peak width increases, the activation energy and the pre-exponential factor decreases except only for CS-MWD-300 and CS-CD-300. This can be correlated to the woody nature of the cotton stalks which makes its behavior to microwave drying different from the other agricultural biomasses.

### 3.2 DTA results

The DTA test provides information regarding the heat flow either to or from the biomass during its pyrolysis indicating whether the reaction is endothermic or exothermic. Figure 6 shows the DTA results for all samples. Figure 6 confirms that the degradation reaction of the biomass is endothermic because of the resulting negative values. There exist mainly three peaks for almost all the samples. The first endothermic peak occurred at approximately 100–200 °C due to the evaporation of the moisture content and interlayer crystal water [15], overlapping with the early stages of the hemicellulose decomposition. It is noticed that the higher the first peak, the more the moisture content of the sample. This first peak is the highest for all biomasses due to the high heat of evaporation of the water.

The second one is in the range from 250–400 °C and is attributed to the complete hemicellulose and partial cellulose degradation which accompanies the release of volatiles [58, 59]. The second peak for all samples is higher for mildly torrefied samples at 250 °C than the severely torrefied samples at 300 °C regardless of the drying method. This totally agrees with the above kinetic results because the remaining amount of hemicellulose significantly decreases at higher torrefaction temperatures resulting in lower heat peaks. Figure 6 shows that for RS, RH, and SC, the second peak is always lower when torrefied at 300 °C regardless of the drying method. This indicates that they have lower hemicellulose content. Whereas for CS, due to its woody nature, CS-MWD-300 has higher remaining hemicellulose content than CS-CD-250 as shown from the first peak in Fig. 6d. Figure 6 shows that MWD conserves more hemicellulose inside the biomass when they are consequently torrefied compared to CD except only for severely torrefied RH; however, the difference is minor.

The third peak starts from approximately 500–800 °C. This peak accounts for the degradation of the remaining cellulose and lignin in the remaining char [58]. At 250 °C torrefaction, MWD increases the cellulose and lignin contents of RS and RH, while it decreases them for SC and CS. At 300 °C torrefaction, MWD increases the lignin contents for RS and SC, hence, the wide temperature reactivity span [60], while it decreases them for RH and CS.

Figure 7 shows the total heat flow during each sample's decomposition across the temperature range from 0 to 800 °C. It is calculated by integrating the area under each of the DTA curves shown in Fig. 6. The value of heat flow varied from one biomass to another due to different moisture, hemicellulose, cellulose, and lignin contents. It is evident that all MWD samples require more heat to decompose compared to their respective CD ones regardless of the torrefaction temperature. This is due to the aggressive nature of MWD which ruptures the inner passages of the biomass. This creates larger voids inside the samples which reduces the coefficient of heat transfer inside the sample making it require more heat input to fully decompose. The ruptured surface also increases the overall surface area of the samples making it lose more heat to the surrounding and increasing the overall heat input to the sample. All samples torrefied at 300 °C require an amount of total heat lower than the ones torrefied at 250 °C except only for CS-MWD-300 due to its woody nature.

### 3.3 BET results

The effect of torrefaction temperature (relative to 250 °C) and drying method on the BET parameters as percent change are presented in Fig. 8a, b, respectively. These percentages are calculated for each one of the three BET parameters presented in Table 2 for both RS and CS as mentioned in section 2.4.

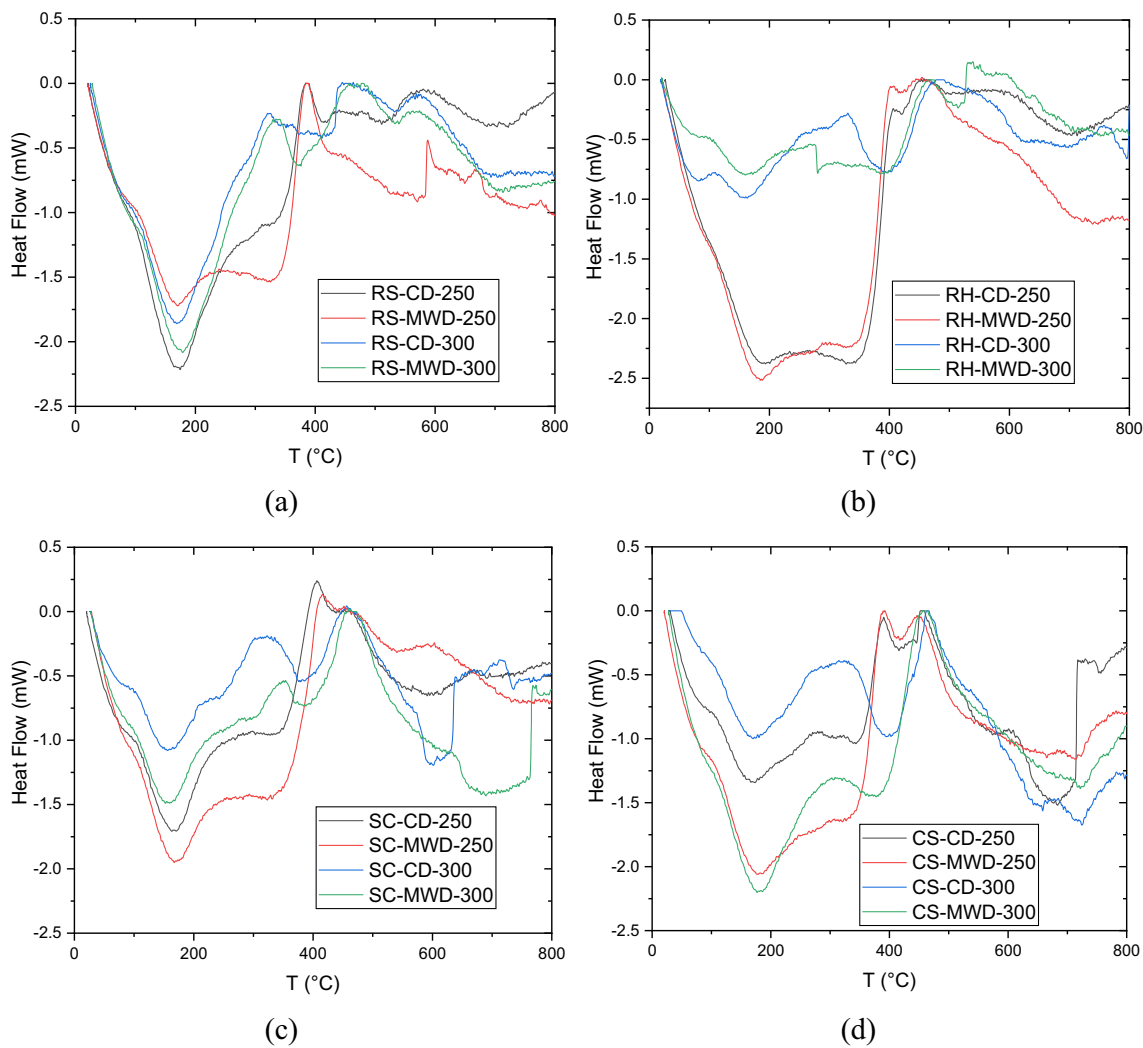


Fig. 6 DTA results for (a) Rice Straw, (b) Rice Husk, (c) Sugarcane Bagasse and (d) Cotton Stalks

For CS, MWD decreased all these BET parameters, regardless of the torrefaction temperature. At 250 °C torrefaction for CS, MWD did not show significant effect on the BET parameters due to the stiff woody nature of the CS and its low crystallinity as shown in Fig. 8b. At 300 °C torrefaction, MWD had a more noticeable effect; however, the percentage decrease in the BET characteristics was much less than RS. This decrease was 5, 61, and 63% for the BET surface area, mean pore diameter, and the total pore volume, respectively. This indicates that MWD increases the porosity of RS making it more suitable for adsorption applications and for soil remediation. The higher surface area to weight ratio means more available adsorption sites per mass [42]. However, it should not be used as fuel because it will have high moisture uptake which will reduce its quality in addition to its lower carbon content and heating value as stated in the authors’ previous work [19]. In the case of CS, MWD decreases its porosity and increases its heating value and carbon content making it better suited as fuel.

It is noticed that as the torrefaction temperature increases, the absolute values of the BET surface area

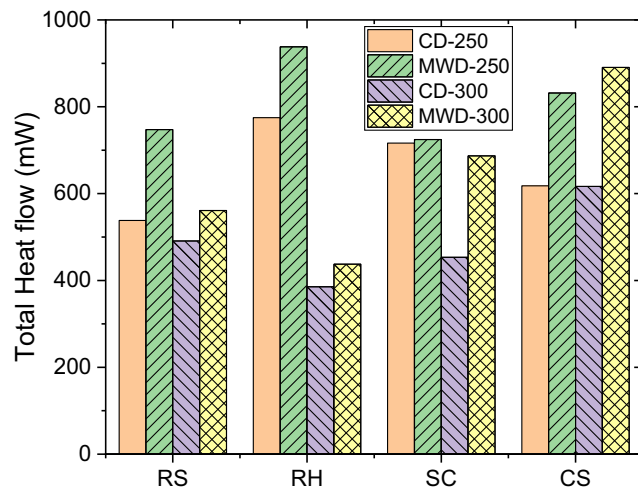
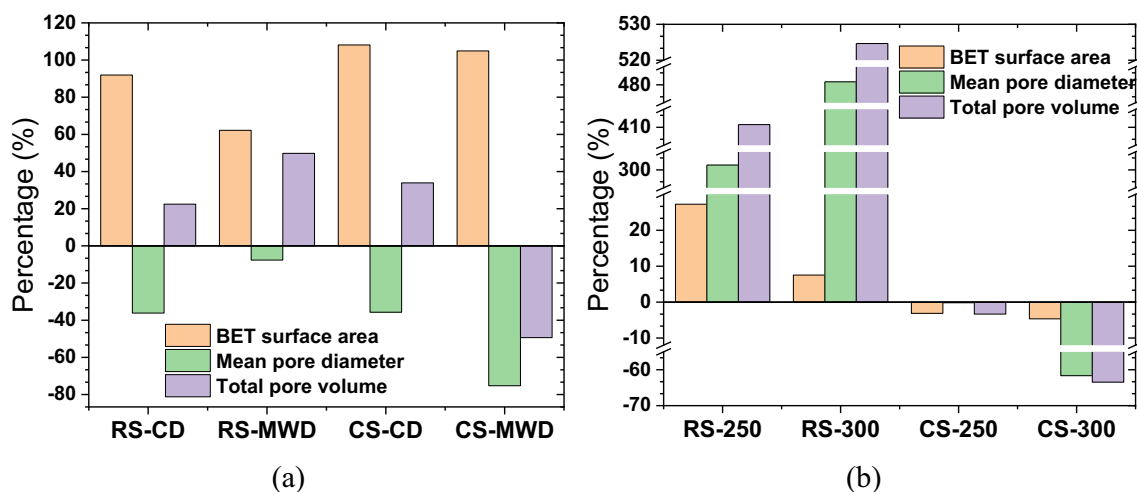


Fig. 7 Total heat flow for biomass decomposition



**Fig. 8** The percentage change in the BET parameters of the RS and CS due to (a) effect of torrefaction temperature at the same drying method and (b) effect of MWD at the same torrefaction temperature

and the total pore volume increase, while the mean pore diameter decreases. This is true for all the samples regardless of the drying method except only for the total pore volume for the MWD torrefied CS as seen in Fig. 8a. This negative temperature coefficient can be attributed to the woody nature of the CS which reduced the overall pore volume at higher torrefaction temperatures. For the same torrefaction temperature, the BET behavior of RS which represents agricultural biomass to MWD is the opposite to the behavior of CS which represents the woody biomass. This is clearly seen in Fig. 8b. For RS, MWD increased the BET surface area by 27 and 7.5%, mean pore diameter by 300 and 480% and the total pore volume by 410 and 524% for mildly and severely torrefied samples, respectively. This high percentage increase can be attributed to the very high crystallinity of the RS [19].

## 4 Conclusion

The effect of microwave drying and torrefaction temperature on the produced biochar from rice straw, rice husk, sugarcane bagasse, and cotton stalks has been investigated; the results revealed numerous effects on the biochar's kinetic parameters and physical structure. As the torrefaction temperature increases, the onset, offset and peak temperatures, and the peak width increase regardless of the drying method, while the absolute maximum decomposition rate  $DTG_{max}$  decreases. MWD increases both  $T_{onset}$  and  $T_{offset}$  when torrefied at 250 °C, while the opposite occurs at 300 °C. MWD reduces the peak width at all torrefaction temperatures for RS, SC, and CS, while the opposite occurs for RH. At 250 °C torrefaction temperature, MWD increased both the absolute value of  $DTG_{max}$  and  $T_{peak}$  for RS, SC, and CS, while the opposite occurs for RH. At 300 °C torrefaction, MWD decreased  $T_{peak}$  for all

**Table 2** BET surface area and characteristics of pore structure for RS and CS

Biomass	Torrefaction temp. (°C)	Drying method	BET surface area $a_{s,BET}$ ( $m^2 \cdot g^{-1}$ )	Mean pore diameter (nm)	Total pore volume ( $p/p_0 = 0.99$ ) ( $cm^3 \cdot g^{-1}$ )
RS	250	CD	1.044	106.37	0.028
		MWD	1.329	426.9	0.142
	300	CD	2.004	67.87	0.034
		MWD	2.155	394.2	0.212
CS	250	CD	0.455	265.29	0.030
		MWD	0.441	264.77	0.029
	300	CD	0.948	170.63	0.040
		MWD	0.904	65.43	0.015

biomasses, decreased the absolute value of  $DTG_{max}$  for RS and CS only and increased  $DTG_{max}$  for RH and SC.

Direct Arrhenius (DA) and Coats and Redfern (CR) methods are used to calculate the activation energy and pre-exponential factor. The best fit reaction order is in the range from 0.8 to 1.3 and from 1.7 to 2 for DA and CR methods, respectively. All activation energy and pre-exponential factor values obtained from CR method are larger than their respective values from the DA method. As the torrefaction temperature increases, both  $E$  and  $A$  decrease. At 250 °C torrefaction, MWD increased both  $E$  and  $A$  for RS, SC, and CS, while the opposite occurred for RH regardless of the kinetic model used. The same happened when torrefied at 300 °C with CR method only. Whereas, both  $A$  and  $E$  decreased with DA method for CS-MWD-300. RS-CD-300 is the easiest one to react as it has the lowest values of  $E$  and  $\ln(A)$ , while SC-MWD-250 is the hardest as it has the maximum values of  $E$  and  $\ln(A)$ .

From the DTA results, MWD kept more hemicellulose inside all biomasses at each torrefaction temperature except only to the severely torrefied RH. MWD increased the total heat flow required to decompose all the samples, regardless of the torrefaction temperature. As the torrefaction temperature increases, the total heat flow decreases for RS, RH, and SC, while it increases for CS due to its woody nature.

MWD increased the porosity of RS making it most suited to be used as activated carbon for adsorption applications or as a soil fertilizer. On the other hand, MWD decreased the porosity of CS making it most suited as fuel. As the torrefaction temperature increases, BET surface area and the total pore volume increased, while the mean pore diameter decreased regardless of the drying method.

## References

- Kanwal S, Chaudhry N, Munir S, Sana H (2019) Effect of torrefaction conditions on the physicochemical characterization of agricultural waste (sugarcane bagasse). *Waste Manag* 88:280–290
- Chan KY, Van Zwieten L, Meszaros I, Downie A, Joseph S (2008) Agronomic values of greenwaste biochar as a soil amendment. *Soil Res* 45(8):629–634
- Nyuykong LP, Djongyang N, Venasius LW, Adeneyi FJ (2015) An efficient method for electrical earth resistance reduction using biochar. *Int J Energy Power Eng* 4(2):65–70
- Ren X, Sun H, Wang F, Cao F (2016) The changes in biochar properties and sorption capacities after being cultured with wheat for 3 months. *Chemosphere* 144:2257–2263
- Gan YY, Ong HC, Show PL, Ling TC, Chen W-H, Yu KL, Abdullah R (2018) Torrefaction of microalgal biochar as potential coal fuel and application as bio-adsorbent. *Energy Convers Manag* 165:152–162
- Zhou J, Liu Y, Han Y, Jing F, Chen J (2019) Bone-derived biochar and magnetic biochar for effective removal of fluoride in groundwater: Effects of synthesis method and coexisting chromium. *Water Environ Res* 91(7):588–597
- Brachi P (2019) Synthesis of fluorescent carbon quantum dots (CQDs) through the mild thermal treatment of agro-industrial residues assisted by  $\gamma$ -alumina. *Biomass Convers Biorefinery*. <https://doi.org/10.1007/s13399-019-00503-4>
- Zhu X, Luo Z, Diao R, Zhu X (2019) Combining torrefaction pretreatment and co-pyrolysis to upgrade biochar derived from bio-oil distillation residue and walnut shell. *Energy Convers Manag* 199:111970
- Tapasvi D, Khalil R, Skreiberg Ø, Tran K-Q, Grønli M (2012) Torrefaction of Norwegian birch and spruce: an experimental study using macro-TGA. *Energy Fuel* 26(8):5232–5240
- Acharya B, Sule I, Dutta A (2012) A review on advances of torrefaction technologies for biomass processing. *Biomass Convers Biorefinery* 2(4):349–369
- Várhegyi G, Bobály B, Jakab E, Chen H (2010) Thermogravimetric study of biomass pyrolysis kinetics. a distributed activation energy model with prediction tests. *Energy Fuel* 25(1):24–32
- Brachi P, Miccio F, Miccio M, Ruoppolo G (2016) Torrefaction of tomato peel residues in a fluidized bed of inert particles and a fixed-bed reactor. *Energy Fuel* 30(6):4858–4868
- Brachi P, Miccio F, Miccio M, Ruoppolo G (2015) Isoconversional kinetic analysis of olive pomace decomposition under torrefaction operating conditions. *Fuel Process Technol* 130:147–154
- Zhang L, Li S, Ding H, Zhu X (2019) Two-step pyrolysis of corn-cob for value-added chemicals and high-quality bio-oil: effects of alkali and alkaline earth metals. *Waste Manag* 87:709–718
- Tabakaev R, Kanipa I, Astafev A, Dubinin Y, Yazykov N, Zavorin A, Yakovlev V (2019) Thermal enrichment of different types of biomass by low-temperature pyrolysis. *Fuel* 245:29–38
- Sousa N, Azevedo JL (2016) Model simplifications on biomass particle combustion. *Fuel* 184:948–956
- Stefanidis G, Stankiewicz A (2016) Alternative energy sources for green chemistry. *Royal Society of Chemistry*
- Wang X, Chen H, Luo K, Shao J, Yang H (2007) The influence of microwave drying on biomass pyrolysis. *Energy Fuel* 22(1):67–74
- Amer M, Nour M, Ahmed M, Ookawara S, Nada S, Elwardany A (2019) The effect of microwave drying pretreatment on dry torrefaction of agricultural biomasses. *Bioresour Technol* 286:121400–121400
- Gai C, Dong Y, Zhang T (2013) The kinetic analysis of the pyrolysis of agricultural residue under non-isothermal conditions. *Bioresour Technol* 127:298–305
- Silva JE, Calixto GQ, de Almeida CC, Melo DM, Melo MA, Freitas JC, Braga RM (2019) Energy potential and thermogravimetric study of pyrolysis kinetics of biomass wastes. *J Therm Anal Calorim* 137(5):1635–1643
- Cai J, Xu D, Dong Z, Yu X, Yang Y, Banks SW, Bridgwater AV (2018) Processing thermogravimetric analysis data for isoconversional kinetic analysis of lignocellulosic biomass pyrolysis: case study of corn stalk. *Renew Sust Energy Rev* 82:2705–2715
- Papari S, Hawboldt K (2015) A review on the pyrolysis of woody biomass to bio-oil: focus on kinetic models. *Renew Sust Energy Rev* 52:1580–1595
- Dacres OD, Tong S, Li X, Zhu X, Edreis EM, Liu H, Luo G, Worasuwannarak N, Kerdsuwan S, Fungtamman B (2019) Pyrolysis kinetics of biomasses pretreated by gas-pressurized torrefaction. *Energy Convers Manag* 182:117–125
- Garba MU, Inalegwu A, Musa U, Aboje AA, Kovo AS, Adeniyi DO (2018) Thermogravimetric characteristic and kinetic of catalytic co-pyrolysis of biomass with low- and high-density polyethylenes. *Biomass Convers Biorefinery* 8(1):143–150

26. Ashraf A, Sattar H, Munir S (2019) A comparative applicability study of model-fitting and model-free kinetic analysis approaches to non-isothermal pyrolysis of coal and agricultural residues. *Fuel* 240:326–333
27. Burnham AK (2017) *Global chemical kinetics of fossil fuels. How to model maturation and pyrolysis* Springer International Publishing AG
28. Aboyade AO, Carrier M, Meyer EL, Knoetze JH, Görgens JF (2012) Model fitting kinetic analysis and characterisation of the devolatilization of coal blends with corn and sugarcane residues. *Thermochim Acta* 530:95–106
29. Kreutter W, Liu Z, McNamara PJ, Singer S (2019) Kinetic analysis of dried biosolids pyrolysis. *Energy Fuel*
30. Hameed S, Sharma A, Pareek V, Wu H, Yu Y (2019) A review on biomass pyrolysis models: kinetic, network and mechanistic models. *Biomass Bioenergy* 123:104–122
31. El-Sayed SA, Mostafa M (2014) Pyrolysis characteristics and kinetic parameters determination of biomass fuel powders by differential thermal gravimetric analysis (TGA/DTG). *Energy Convers Manag* 85:165–172
32. Huang Y, Chen W, Chiueh P, Kuan W, Lo S (2012) Microwave torrefaction of rice straw and pennisetum. *Bioresour Technol* 123: 1–7
33. Elbaz AM, Gani A, Hourani N, Emwas A-H, Sarathy SM, Roberts W (2015) TG/DTG, FT-ICR mass spectrometry, and NMR spectroscopy study of heavy fuel oil. *Energy Fuel* 29(12):7825–7835
34. Khateeb AA, Elbaz AM, Guida P, Roberts WL (2018) Influence of asphaltene concentration on the combustion of a heavy fuel oil droplet. *Energy Fuel* 32(12):12981–12991
35. Jayaraman K, Kok MV, Gokalp I (2017) Thermogravimetric and mass spectrometric (TG-MS) analysis and kinetics of coal-biomass blends. *Renew Energy* 101:293–300
36. Mallick D, Bora BJ, Barbhuiya SA, Banik R, Garg J, Sarma R, Gogoi AK (2019) Detailed study of pyrolysis kinetics of biomass using thermogravimetric analysis. In: *AIP Conference Proceedings*, vol 1. AIP Publishing, p 020014
37. Chen C, Yang S, Bu X (2019) Microwave drying effect on pyrolysis characteristics and kinetics of microalgae. *BioEnergy Res* 12(2): 400–408
38. Liang J, Yu Z, Chen L, Fang S, Ma X (2019) Microwave pretreatment power and duration time effects on the catalytic pyrolysis behaviors and kinetics of water hyacinth. *Bioresour Technol* 286: 121369
39. Boycheva S, Zgureva D, Vassilev V (2013) Kinetic and thermodynamic studies on the thermal behaviour of fly ash from lignite coals. *Fuel* 108:639–646
40. El-Sayed SA, Mostafa ME (2015) Kinetic parameters determination of biomass pyrolysis fuels using TGA and DTA techniques. *Waste Biomass Valorization* 6(3):401–415
41. Basu P (2010) *Biomass gasification and pyrolysis: practical design and theory*. Academic press
42. Pandey A (2011) *Biofuels: alternative feedstocks and conversion processes*. Academic Press
43. Basu P (2018) *Biomass gasification, pyrolysis and torrefaction: practical design and theory*. Academic press
44. Pallarés J, González-Cencerrado A, Arauzo I (2018) Production and characterization of activated carbon from barley straw by physical activation with carbon dioxide and steam. *Biomass Bioenergy* 115:64–73
45. Yan W, Perez S, Sheng K (2017) Upgrading fuel quality of moso bamboo via low temperature thermochemical treatments: dry torrefaction and hydrothermal carbonization. *Fuel* 196:473–480
46. Pure IUo, Division ACAC (1997) *Compendium of analytical nomenclature: definitive rules 1997*. International Union of Pure and Applied Chemistry,
47. Coats A, Redfern J-P (1965) Kinetic parameters from thermogravimetric data. II. *J Polym Sci B Polym Lett* 3(11):917–920
48. Coats AW, Redfern J (1964) Kinetic parameters from thermogravimetric data. *Nature* 201(4914):68
49. Edreis EM, Yao H (2016) Kinetic thermal behaviour and evaluation of physical structure of sugar cane bagasse char during non-isothermal steam gasification. *J Mater Res Technol* 5(4):317–326
50. Chen W-H, Lu K-M, Tsai C-M (2012) An experimental analysis on property and structure variations of agricultural wastes undergoing torrefaction. *Appl Energy* 100:318–325
51. Zhao C, Jiang E, Chen A (2017) Volatile production from pyrolysis of cellulose, hemicellulose and lignin. *J Energy Inst* 90(6):902–913
52. Huang Y-F, Cheng P-H, Chiueh P-T, Lo S-L (2017) Leucaena biochar produced by microwave torrefaction: fuel properties and energy efficiency. *Appl Energy* 204:1018–1025
53. He Q, Ding L, Gong Y, Li W, Wei J, Yu G (2019) Effect of torrefaction on pinewood pyrolysis kinetics and thermal behavior using thermogravimetric analysis. *Bioresour Technol* 280:104–111
54. Özsın G, Pütün AE (2019) TGA/MS/FT-IR study for kinetic evaluation and evolved gas analysis of a biomass/PVC co-pyrolysis process. *Energy Convers Manag* 182:143–153
55. Kai X, Meng Y, Yang T, Li B, Xing W (2019) Effect of torrefaction on rice straw physicochemical characteristics and particulate matter emission behavior during combustion. *Bioresour Technol* 278:1–8
56. Ceylan S, Kazan D (2015) Pyrolysis kinetics and thermal characteristics of microalgae *Nannochloropsis oculata* and *Tetraselmis* sp. *Bioresour Technol* 187:1–5
57. Bhuiyan MTR, Hirai N, Sobue N (2000) Changes of crystallinity in wood cellulose by heat treatment under dried and moist conditions. *J Wood Sci* 46(6):431–436
58. Jiang L, Yuan X, Xiao Z, Liang J, Li H, Cao L, Wang H, Chen X, Zeng G (2016) A comparative study of biomass pellet and biomass-sludge mixed pellet: energy input and pellet properties. *Energy Convers Manag* 126:509–515
59. Barmina I, Kolmickovs A, Valdmanis R, Vostrikovs S, Zake M (2018) Thermo-Chemical Conversion of Microwave Activated Biomass Mixtures. In: *IOP Conference Series: Materials Science and Engineering*, vol 1. IOP Publishing, p 012018
60. Malucelli L, Carneiro J, Vasconcelos E, Magalhães W, Murakami F, Carvalho Filho M (2019) Energetic potential of pyrolyzed biomass from different sources: a comparative study. *J Therm Anal Calorim*. <https://doi.org/10.1007/s10973-019-09061-3>

**Publisher's Note** Springer Nature remains neutral with regard to jurisdictional claims in published maps and institutional affiliations.